PHYSICAL REVIEW C **86**, 041603(R) (2012)

Self-consistent microscopic description of neutron scattering by ^{16}O based on the continuum particle-vibration coupling method

Kazuhito Mizuyama* and Kazuyuki Ogata
Research Center for Nuclear Physics, Osaka University, Ibaraki 567-0047, Japan
(Received 9 October 2012; published 22 October 2012)

The microscopic description of neutron scattering by ^{16}O below 30 MeV is carried out by means of the continuum particle-vibration coupling (cPVC) method with the Skyrme nucleon-nucleon (NN) effective interaction. In the cPVC method, a proper boundary condition on a nucleon in continuum states is imposed, which enables one to evaluate the transition matrix in a straightforward manner. Experimental data of the total and total-elastic cross sections are reproduced quite well by the cPVC method. An important feature of the result is the fragmentation of the single-particle resonance into many peaks as well as the shift of its centroid energy. Thus, some part of the fine structure of the experimental cross sections at lower energies is well described by the cPVC framework. The cPVC method based on a real NN effective interaction is found to successfully explain about 85% of the reaction cross section, through explicit channel-coupling effects.

DOI: 10.1103/PhysRevC.86.041603 PACS number(s): 21.60.Jz, 24.10.Eq, 24.10.Ht, 25.60.Bx

Description of nucleon-nucleus (NA) elastic scattering based on the fundamental nucleon-nucleon (NN) interaction is one of the most challenging subjects of nuclear reaction studies, and is crucial to the exploration of unstable nuclei, for which phenomenological optical potentials have not been established. The most essential quantity for this subject is the imaginary part W of the optical potential, which is responsible for a loss of the incident flux due to the existence of nonelastic channels. Reliability of W can be judged by comparing the resulting reaction cross section σ_R with experimental data.

One of the most successful approaches to this goal is the folding model based on a complex effective NN interaction and a phenomenological or microscopic nuclear density. In Ref. [1], for example, the folding model calculation with no free parameter is shown to reproduce well the differential cross sections and spin observables for proton elastic scattering on ^{12}C, ^{16}O, ^{40}Ca, ^{90}Zr, and ^{208}Pb at 65–200 MeV, as well as σ_R of neutrons on these targets at 20–800 MeV. The agreement is at almost the same level as that of the well-established Dirac phenomenology [2,3]. Many studies in this direction have successfully been done with the coordinate-space representation [4–7] and the momentum-space representation [8]. Nowadays, the microscopic description of nucleus-nucleus (AA) scattering has become a hot topic [9]. In all these models, W comes from the imaginary part of the effective NN interaction, for which a Brückner g matrix evaluated in infinite nuclear matter is often adopted. Despite the great success of this folding-model approach, it is quite obvious that the use of the g matrix is not feasible for low-energy scattering, because individual energy levels of the $N + A$ system near the nucleon threshold strongly affect the scattering process.

An alternative approach to the microscopic description of NA elastic scattering is many-body calculation of the $N + A$ system including channel couplings to the continuum states. In this approach, a NN effective interaction with no imaginary part is used, and W is generated through the coupling to nonelastic channels that are explicitly taken into account. One of the most suitable models for this purpose will be the particle-vibration coupling (PVC) method, which describes collective vibrations and single-particle motion of individual nucleons simultaneously. In a recent paper [10], the microscopic continuum PVC (cPVC) method was proposed and applied to studies on single-particle (sp) structures in ^{40}Ca, ^{208}Pb, and ^{24}O. In general, the sp states of a nucleus A are observed in excitation energy spectra in the neighboring $A \pm 1$ nuclei. It was shown in Ref. [10] that the cPVC method describes quite well the fragmentation of the sp hole and particle states as well as the shift of those centroid energies, in good agreement with experimental data. These are distinguished features of sp states that are not taken into account in the standard Hartree-Fock (HF) picture.

The cPVC method is based on the self-consistent microscopic HF and the continuum random-phase approximation (RPA) [11,12] with the Skyrme effective interaction. In this framework, the microscopic nucleon optical potential is characterized by the nucleon self-energy corresponding to specific energy E in the asymptotic region of the $N + A$ system; E can be interpreted as the incident energy of the nucleon on the target nucleus A in the optical model picture. A great advantage of the cPVC method to other existing PVC models [13–16] is, as emphasized in Ref. [10], the proper treatment of the continuum with imposing an explicit boundary condition on a nucleon in a continuum state. Therefore, it is quite promising that the cPVC method can be applied to studies on reaction observables for which boundary conditions play essential roles in general.

In this Rapid Communication, we apply the cPVC method to the neutron scattering on ^{16}O below 30 MeV. We see how the cPVC method can describe the absolute values and energy dependence of σ_R in particular. Important aspects of the present study, in comparison with the preceding works [16,17] along the same line, are as follows. First, we treat the continuum

*mizukazu147@gmail.com

explicitly as mentioned above. Second, we include a very large model space (various phonon states up to 60 MeV) as described below. Third, we are interested in the structures, i.e., nontrivial energy dependence, of σ_R due to the PVC, expected to appear at quite lower incident energies.

In the cPVC framework, the scattering wave function of neutron $\Psi_{\rm PVC}(\boldsymbol{r}\sigma, \boldsymbol{k})$ from A, with the relative coordinate $\boldsymbol{r}$, the intrinsic coordinate σ due to the spin degrees of freedom, and the relative wave number $\boldsymbol{k}$ in the asymptotic region, is described by the following Lippmann-Schwinger equation:

$$\begin{aligned}\Psi^{(+)}_{\rm PVC}(\boldsymbol{r}\sigma, \boldsymbol{k}) &= \phi_F(\boldsymbol{r}\sigma, \boldsymbol{k}) + \sum_{\sigma'\sigma''}\int\!\!\int d\boldsymbol{r}' d\boldsymbol{r}'' G^{(+)}(\boldsymbol{r}\sigma, \boldsymbol{r}'\sigma'; E) \\ &\times [v(\boldsymbol{r}'\sigma')\delta(\boldsymbol{r}' - \boldsymbol{r}'')\delta_{\sigma'\sigma''} + \Sigma(\boldsymbol{r}'\sigma', \boldsymbol{r}''\sigma''; E)] \\ &\times \phi_F(\boldsymbol{r}''\sigma'', \boldsymbol{k}), \end{aligned} \tag{1}$$

where ϕ_F denotes the neutron free wave and $v(\boldsymbol{r}'\sigma')$ is the HF one-body mean-field potential. The PVC Green's function and the corresponding self-energy are denoted by $G^{(+)}(\boldsymbol{r}\sigma, \boldsymbol{r}'\sigma'; E)$ and $\Sigma(\boldsymbol{r}'\sigma', \boldsymbol{r}''\sigma''; E)$, respectively. With the partial wave expansion, one may find that the transition matrix (T matrix) of the elastic scattering is given by

$$\begin{aligned}T^{\rm PVC}_{lj}(E) = \lim_{\to\infty} \frac{2i}{r h^{(+)}_l(kr)} \int\!\!\int dr' dr'' r'' G^{(+)}_{lj}(rr'; E) \\ \times [v_{lj}(r')\delta(r' - r'') + \Sigma_{lj}(r'r''; E)] j_l(kr''), \end{aligned} \tag{2}$$

where l (j) represents the orbital angular momentum (total single-particle spin) of the neutron, and $h^{(+)}_l(kr)$ and $j_l(kr)$ are, respectively, the spherical Hankel function with the outgoing asymptotics and the spherical Bessel function. Explicit expressions of $G^{(+)}$ and Σ are given by Eqs. (6) and (7) of Ref. [10], respectively. Note that we use E for the relative energy between neutron and A, which is denoted by ω in Ref. [10]. Furthermore, we put (+) in the superscript of $\Psi_{\rm PVC}$, G, and G_{lj}, to explicitly represent that these functions satisfy the outgoing boundary condition. We solve a Dyson equation, Eq. (10) of Ref. [10], to obtain G_{lj}, and hence $T^{\rm PVC}_{lj}$. All other details can be found in Ref. [10].

The differential elastic cross section $d\sigma/d\Omega$ is given by

$$\frac{d\sigma}{d\Omega} = |\mathcal{F}(\theta)|^2 + |\mathcal{G}(\theta)|^2, \tag{3}$$

where

$$\mathcal{F}(\theta) = \frac{1}{2ik}\sum_{lj}\frac{2j+1}{2}\{-iT_{lj}(E)\}P_l(\cos\theta), \tag{4}$$

$$\begin{aligned}\mathcal{G}(\theta) = \frac{\sin\theta}{2k}\sum_{l(\neq 0)j}\frac{2j+1}{2}\frac{j(j+1) - l(l+1) - 3/4}{l(l+1)} \\ \times\{-iT_{lj}(E)\}P'_l(\cos\theta). \end{aligned} \tag{5}$$

Here, P_l and P'_l are, respectively, the Legendre polynomial and its derivative with respect to $\cos\theta$. The total cross section $\sigma_{\rm tot}$ and the total-elastic cross section $\sigma_{\rm el}$ are given by

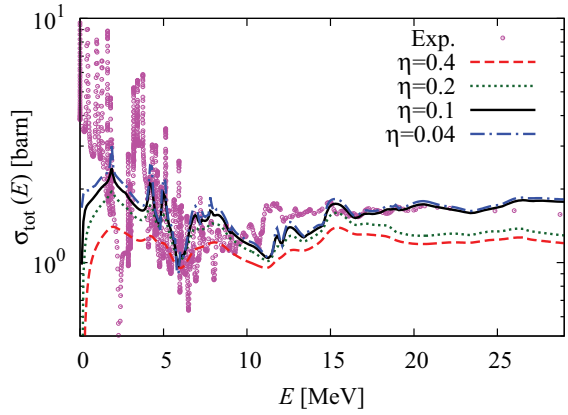

FIG. 1. (Color online) Total cross section of neutron scattering by ^{16}O, as a function of the incident energy. The dashed, dotted, solid, and dash-dotted lines show the results with $\eta = 0.4$, 0.2, 0.1, and 0.04 MeV, respectively. Experimental data are taken from Ref. [19].

$$\sigma_{\rm tot}(E) = \sum_{lj}\frac{2\pi}{k^2}\frac{2j+1}{2}[{\rm Im}\ T_{lj}(E)] \equiv \sum_{lj}\sigma_{{\rm tot};lj}(E), \tag{6}$$

$$\sigma_{\rm el}(E) = \sum_{lj}\frac{\pi}{k^2}\frac{2j+1}{2}|T_{lj}(E)|^2 \equiv \sum_{lj}\sigma_{{\rm el};lj}(E). \tag{7}$$

The reaction cross section σ_R is defined by

$$\sigma_R(E) = \sigma_{\rm tot}(E) - \sigma_{\rm el}(E). \tag{8}$$

As one may see from Eqs. (1) and (2), the self-energy Σ serves as a dynamical polarization potential. Therefore, the imaginary part W of the optical potential comes from Σ, which takes into account the coupling within the Skyrme continuum-RPA response function and the HF Green's function [10]. Note that we explicitly treat the nonlocality of Σ, whereas it was approximately localized in the previous work [16]. The HF T matrix can be obtained by

$$\begin{aligned}T^{\rm HF}_{lj}(E) = \lim_{r\to\infty}\frac{2i}{r h^{(+)}_l(kr)}\int dr' r' G^{(+)}_{0,lj}(rr'; E) \\ \times v_{lj}(r') j_l(kr'), \end{aligned} \tag{9}$$

where $G^{(+)}_{0,lj}$ means the HF Green's function.

In the present calculation, we adopt the Skyrme NN effective interaction SkM* [18]. Note that, in contrast to Ref. [17], we do not introduce any other interactions to the calculation of scattering observables; i.e., a fully consistent treatment of the effective interaction is carried out. For the cPVC calculation, as in Ref. [10], the orbital angular momentum cutoff for the unoccupied continuum states is set at $l_{\rm cut} = 7\hbar$, and we include phonons associated with the multipolarities λ^π of 2^+, 3^-, 4^+, and 5^-, up to 60 MeV of the RPA excitation energy. We choose the Fermi momentum $k_F = 1.33$ fm^{-1} for the residual force in the self-energy function of the PVC calculation. The radial mesh size is $\Delta r = 0.2$ fm and the maximum value of r is set to 20 fm, to obtain the T matrix by Eq. (2).

First, we show in Fig. 1 the η dependence of $\sigma_{\rm tot}(E)$ of neutron scattering by ^{16}O; η is a parameter introduced in the evaluation of Green's function and the RPA response function [10], and corresponds to the resolution scale of E. The dashed,

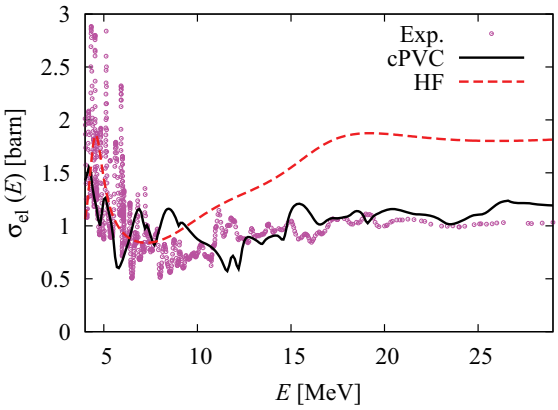

FIG. 2. (Color online) Total-elastic cross section of the neutron scattering by ^{16}O. The solid (dashed) line shows the result of the cPVC method (HF calculation). Experimental data are taken from Ref. [19].

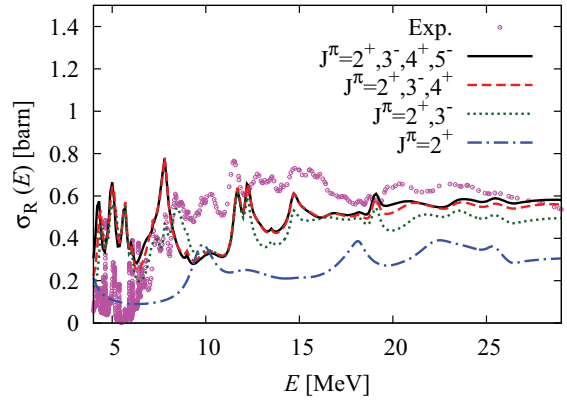

FIG. 3. (Color online) Reaction cross section of neutron for ^{16}O. The solid, dashed, dotted, and dash-dotted lines correspond to the calculation with $\lambda_{max} = 5$, 4, 3, and 2, respectively. Experimental data are taken from Ref. [19].

dotted, solid, and dash-dotted lines show the results with $\eta = 0.4$, 0.2, 0.1, and 0.04 MeV, respectively. Considering the experimental situation, E should be an order of eV, which cannot be achieved because of the computational limitation. As one sees from the figure, however, $\sigma_{tot}(E)$ for $E \geqslant 4.0$ MeV converges at $\eta = 0.1$ MeV. Thus, in the following discussion we use $\eta = 0.1$ MeV and restrict ourselves for $E \geqslant 4.0$ MeV.

In Fig. 1, the solid line reproduces quite well the energy dependence of the experimental data [19] except for $10 \lesssim E \lesssim 15$ MeV. A remarkable feature is the reproduction of the fine structure of $\sigma_{tot}(E)$ in part, which is the benefit of the PVC. It is well known that many peaks in the experimental $\sigma_{tot}(E)$ correspond to the compound resonance. It is quite obvious that the present cPVC calculation cannot describe such peaks. Rather than that, the cPVC method is considered to describe well the so-called doorway states [20]. Keeping this in mind, we see that the present calculation reasonably reproduces the energy dependence of $\sigma_{tot}(E)$. Note that we do not tune any adjustable parameters, although the result can, to some extent, depend on the Skyrme parameters adopted.

Figure 2 shows the $\sigma_{el}(E)$ calculated by the cPVC method (solid line) and the HF calculation (dashed line). Results are plotted in the linear scale. The cPVC method reproduces well the experimental data [19], whereas the HF calculation overshoots them by about 80% above 15 MeV. This shortcoming of the HF calculation is rather trivial because of the absence of the imaginary part of the optical potential; absorption effects become more significant as E, the number of open channels, in fact, increases. It should be noted that the HF calculation gives $\sigma_{el}(E) = \sigma_{tot}(E)$ and hence $\sigma_R(E) = 0$. Another important finding is that the HF result has only one peak around 4.6 MeV, which turns out to be due to the $f_{7/2}$ sp orbit. The cPVC method gives much more complicated shapes of $\sigma_{el}(E)$, as in Fig. 1. This result clearly shows the importance of the PVC in the neutron elastic scattering at low energies.

Next we compare the result of $\sigma_R(E)$ (solid line) with the experimental data [19] in Fig. 3. Again, we plot the result in the linear scale. Although the theoretical $\sigma_R(E)$ slightly undershoots (overshoots) the data for $10 \lesssim E \lesssim 25$ MeV ($E \lesssim 6$ MeV), some peak structure is reproduced well. On the average for $8 \lesssim E \lesssim 30$ MeV, the discrepancy between the theoretical values and experimental data for $\sigma_R(E)$ is about 15%. It should be noted that the present cPVC calculation describes the $\sigma_R(E)$ only though channel-coupling effects, i.e., with no imaginary part of an effective interaction. It will be a remarkable achievement that about 85% of the $\sigma_R(E)$ is successfully explained in this manner. It was shown in Ref. [17] that more than half the $\sigma_R(E)$ for proton scattering on ^{58}Ni, ^{48}Ca, and ^{90}Zr is due to a coupling with the deuteron (transfer) channel. In the present calculation, the deuteron channel seems to play less important roles; it should be remarked that (i) theoretical calculation shows good agreement with data for $E \gtrsim 25$ MeV and (ii) we still have undershooting around 10 MeV, where the (n, d) reaction channel is closed.

In Fig. 3, the dependence of $\sigma_R(E)$ on the maximum multipolarity λ_{max} is also shown. The dashed, dotted, and dash-dotted lines correspond to the calculation with $\lambda_{max} = 4$, 3, and 2, respectively; the solid line represents the full calculation with $\lambda_{max} = 5$. One sees a good convergence at $\lambda_{max} = 4$. Another finding is the role of $\lambda = 3$, which essentially generates the many peaks in $\sigma_R(E)$; $\lambda = 4$ then gives a slight change in the shapes and positions of the peaks.

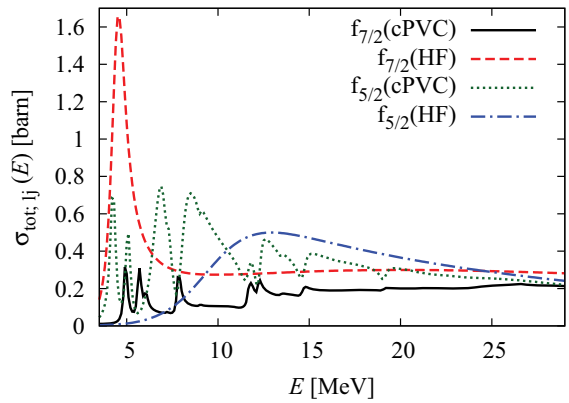

FIG. 4. (Color online) Partial cross sections of σ_{tot}. The solid (dashed) and dotted (dash-dotted) lines represent the results of the $f_{7/2}$ and $f_{5/2}$ orbits obtained by the cPVC method (HF calculation).

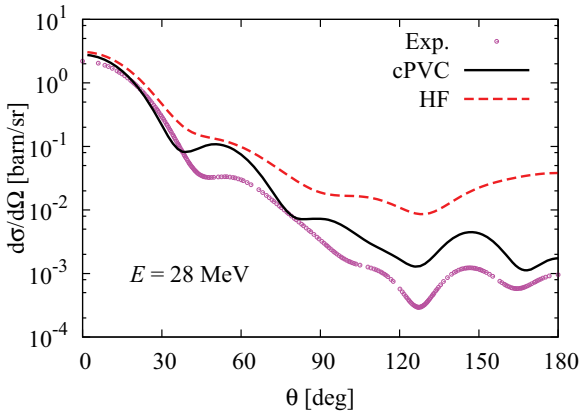

FIG. 5. (Color online) Angular distribution of the neutron elastic cross section by ^{16}O at 28 MeV. The solid (dashed) line shows the result of the cPVC method (HF calculation). Experimental data are taken from Ref. [19].

To see how the PVC gives peaks in the cross section more clearly, we show in Fig. 4 the partial cross sections of $\sigma_{\rm tot}(E)$, $\sigma_{{\rm tot};lj}(E)$ in Eq. (6), for the f orbits. The cPVC (HF) result for the $f_{7/2}$ and $f_{5/2}$ orbits are shown by the solid (dashed) and dotted (dash-dotted) lines, respectively. The dashed line has a resonant peak around 4.6 MeV, which is fragmented by the PVC as shown by the solid line. Similarly, the PVC changes the dash-dotted line to the dotted line, generating nontrivial structures. Thus, the PVC completely changes the shapes of the partial cross sections. Fragmentation of the sp strength function is necessary to explain the energy dependence of experimental data, as shown in Figs. 1–3.

Finally, we show the result of the differential cross section $d\sigma/d\Omega$ in Fig. 5. The cPVC and HF results are denoted by the solid and dashed lines, respectively. The dashed line severely overshoots the data at backward angles. This issue remains for the solid line, although the agreement with the experimental data is significantly improved by including the PVC. This may indicate that the radial dependence of the optical potential is not correctly generated by the present framework; further investigation on this is our future work.

In this study, we applied the continuum particle-vibration coupling (cPVC) method to the calculation of scattering observables, i.e., the total $\sigma_{\rm tot}$, total-elastic $\sigma_{\rm el}$, and reaction σ_R cross sections, of neutrons on the ^{16}O target at 4–30 MeV. The cPVC method describes the single-particle motion and collective vibrations simultaneously, with properly treating the boundary condition of a nucleon in continuum states. This feature makes the calculation of the transition matrix (T matrix) straightforward. We used the Skyrme interaction (SkM*) as an effective nucleon-nucleon (NN) interaction, and included phonon states of ^{16}O up to the 5^- state with excitation energy of 60 MeV. The T matrix is evaluated with the PVC Green's function, which is obtained by solving the Dyson equation. The couplings to various collective states are characterized by the self-energy Σ. Since the cPVC method employs a real NN interaction, the imaginary part of the optical potential purely comes from Σ. In the present framework, σ_R is described as a loss of the incident flux to various channels that are explicitly taken into account.

The results of the present cPVC calculation satisfactorily agree well with experimental data of $\sigma_{\rm tot}$ and $\sigma_{\rm el}$. For σ_R, the cPVC method explains about 85% of the experimental data on average, which will be an important achievement of the mean-field type calculation for neutron scattering. Another remarkable feature of the cPVC result is the fragmentation of a single-particle resonant cross section. This results in good correspondence with some of the peaks observed, probably those due to the doorway states. On the other hand, the Hartree-Fock (HF) calculation was found to give a rather trivial shape of the cross section and severely overshoot $\sigma_{\rm el}$ for $E \gtrsim 10$ MeV. The cPVC method describes the angular distribution of the elastic cross section much better than the HF calculation. However, there still remains a discrepancy at scattering angles larger than 30°. This will be due to an incorrect radial dependence of the optical potential in the cPVC framework.

In the future, we will apply the cPVC method to other reaction systems, including proton scattering. Application to inelastic scattering and photoinduced reactions will also be important. Another important subject is the interaction dependence. The scattering observables can be used as new constraints on the parameters of the Skyrme interaction, determined to reproduce nuclear bound-state properties. In addition to that, as discussed in Ref. [10], further investigation on the treatment of Pauli's principle in the cPVC framework will be necessary.

The authors thank G. Colò, M. Yahiro, and K. Hagino for helpful discussions.

[1] P. K. Deb, B. C. Clark, S. Hama, K. Amos, S. Karataglidis, and E. D. Cooper, Phys. Rev. C **72**, 014608 (2005).
[2] L. Ray, G. W. Hoffmann, and W. R. Coker, Phys. Rep. **212**, 223 (1992).
[3] E. D. Cooper, S. Hama, B. C. Clark, and R. L. Mercer, Phys. Rev. C **47**, 297 (1993).
[4] L. Rikus, K. Nakano, and H. V. von Geramb, Nucl. Phys. A **414**, 413 (1984).
[5] L. Rikus and H. V. von Geramb, Nucl. Phys. A **426**, 496 (1984).
[6] K. Amos, P. J. Dortmans, H. V. von Geramb, S. Karataglidis, and J. Raynal, Adv. Nucl. Phys. **25**, 275 (2000).
[7] P. K. Deb and K. Amos, Phys. Rev. C **62**, 024605 (2000).
[8] S. P. Weppner, Ch. Elster, and D. Huber, Phys. Rev. C **57**, 1378 (1998) and references therein.
[9] T. Furumoto, Y. Sakuragi, and Y. Yamamoto, Phys. Rev. C **78**, 044610 (2008); **79**, 011601(R) (2009); **80**, 044614 (2009).
[10] K. Mizuyama, G. Colò, and E. Vigezzi, Phys. Rev. C **86**, 034318 (2012).

[11] K. Mizuyama, M. Matsuo, and Y. Serizawa, Phys. Rev. C **79**, 024313 (2009).
[12] H. Sagawa, Prog. Theor. Phys. Suppl. **142**, 1 (2001).
[13] G. Colò, H. Sagawa, and P. F. Bortignon, Phys. Rev. C **82**, 064307 (2010).
[14] E. Litvinova and P. Ring, Phys. Rev. C **73**, 044328 (2006).
[15] E. V. Litvinova and A. V. Afanasjev, Phys. Rev. C **84**, 014305 (2011).
[16] V. Bernard and N. Van Giai, Nucl. Phys. A **327**, 397 (1979).
[17] G. P. A. Nobre, F. S. Dietrich, J. E. Escher, I. J. Thompson, M. Dupuis, J. Terasaki, and J. Engel, Phys. Rev. C **84**, 064609 (2011).
[18] J. Bartel, P. Quentin, M. Brack, C. Guet, and H. B. Hakansson, Nucl. Phys. A **386**, 79 (1982).
[19] Data retrieved from the National Nuclear Data Center, Brookhaven National Laboratory Online Data Service, http://www.nndc.bnl.gov/exfor/exfor00.htm.
[20] C. F. Weisskopf, Phys. Today **14**, 18 (1961).